Spontaneous Phase and Morphology Transformations of Anodized Titania Nanotubes Induced by Water at Room Temperature

Daoai Wang,*[,†,‡,||] Lifeng Liu,*[,†,§,||] Fuxiang Zhang,[‡] Kun Tao,[†] Eckhard Pippel,[†] and Kazunari Domen[‡]

[†]Max Planck Institute of Microstructure Physics, Weinberg 2, D-06120 Halle, Germany

[‡]Department of Chemical System Engineering, The University of Tokyo, 7-3-1 Hongo, Bunkyo-ku, Tokyo 113-8656, Japan

[§]International Iberian Nanotechnology Laboratory (INL), 4715-330 Braga, Portugal

S *Supporting Information*

ABSTRACT: We report a spontaneous phase transformation of titania nanotubes induced by water at room temperature, which enables the as-anodized amorphous nanotubes to be crystallized into anatase mesoporous nanowires without any other post-treatments. These mesoporous TiO_2 nanomaterials have a markedly improved surface area, about 5.5 times than that of the as-anodized TiO_2 nanotubes, resulting in a pronounced enhanced photocatalytic activity. The present approach not only allows a flexible control over the morphology of TiO_2 nanostructures but can fundamentally eliminate the need for high temperature operations for crystallizing amorphous TiO_2.

KEYWORDS: TiO_2 nanotubes, phase transformation, mesoporous structures, photocatalyst
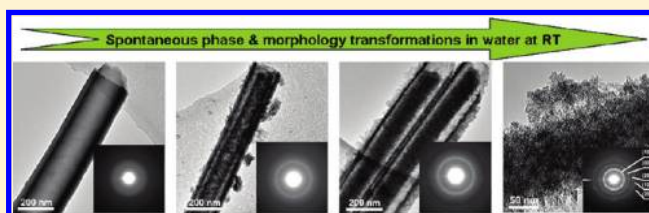
Despite recent remarkable advances in the development of various nonconventional photoactive inorganic semiconductors,[1−8] titania (TiO_2) to date still remains one of the most popular materials for applications in photocatalysis and photovoltaics due to its relatively high efficiency, chemical inertness, good photostability upon irradiation, low cost, and abundance.[9−12] In particular, arrays of one-dimensional (1D) TiO_2 nanostructures such as nanowires (NWs) and nanotubes (NTs) have drawn ever-increasing attention because they not only possess high surface areas but also offer the advantage of directed carrier transport facilitating the collection of photogenerated charge carriers and therefore are expected to be promising high-performance photoanodes for use in both dye-sensitized solar cells (DSCs) and solar fuel production.[13−23] So far, electrochemical oxidation of titanium has been widely considered as a facile, inexpensive, and scalable method for the fabrication of self-organized TiO_2 NT arrays that can exhibit greatly enhanced performances.[11−20] However, nearly all TiO_2 NT arrays fabricated by anodization are amorphous in nature, thus substantially limiting their direct use in many cases, particularly in photocatalysis and DSCs where photoactive crystalline anatase TiO_2 is highly desired. In order to obtain the desired crystalline phase, postheat treatments such as thermal annealing[11,12,24] or hydrothermal processing[25] are generally needed. These post-treatment approaches unexceptionally involve additional energy consumption, which not only are costly but also increase the energy pay-back time in cases where the TiO_2 NTs are used for an energy-harvesting purpose. To overcome this problem, direct fabrication of crystalline TiO_2 NT arrays by anodizing titanium in an electrolyte at moderate temperatures (80−180 °C) or in a polyol

electrolyte has recently been attempted,[26,27] but only limited success was achieved.

On the other hand, it is well-known that improving surface area of TiO_2 nanostructures can also effectively enhance their photocatalytic and photoelectric properties. To this end, several approaches such as creation of mesoporous and/or secondary structures on 1D TiO_2 nanomaterials have been developed.[28−31] However, in most cases, the introduced mesoporous/secondary structures are amorphous and their high surface areas will be compromised in pursuit of a higher degree of crystallinity through high-temperature annealing. Therefore, it is highly desirable to find a low-temperature route to fabricate crystalline anatase TiO_2 nanostructures with a high surface area.

Here we show a simple and effective method to obtain anatase mesoporous TiO_2 NW arrays by just soaking the as-anodized amorphous TiO_2 NTs in water at room temperature. This room-temperature amorphous-anatase phase transformation does not require any extra energy input, additional chemical treatment, and/or the assistance of any other equipment and, therefore, represents a facile and cost-effective route toward crystallization of amorphous TiO_2 materials, which may be of great industrial interest. Moreover, the induced mesopores during the transformation process render the resulting crystalline TiO_2 products a greatly improved surface area, which is beneficial for their use in photocatalysis and DSCs. Additionally, the room-temperature phase transformation process also enables the active crystalline
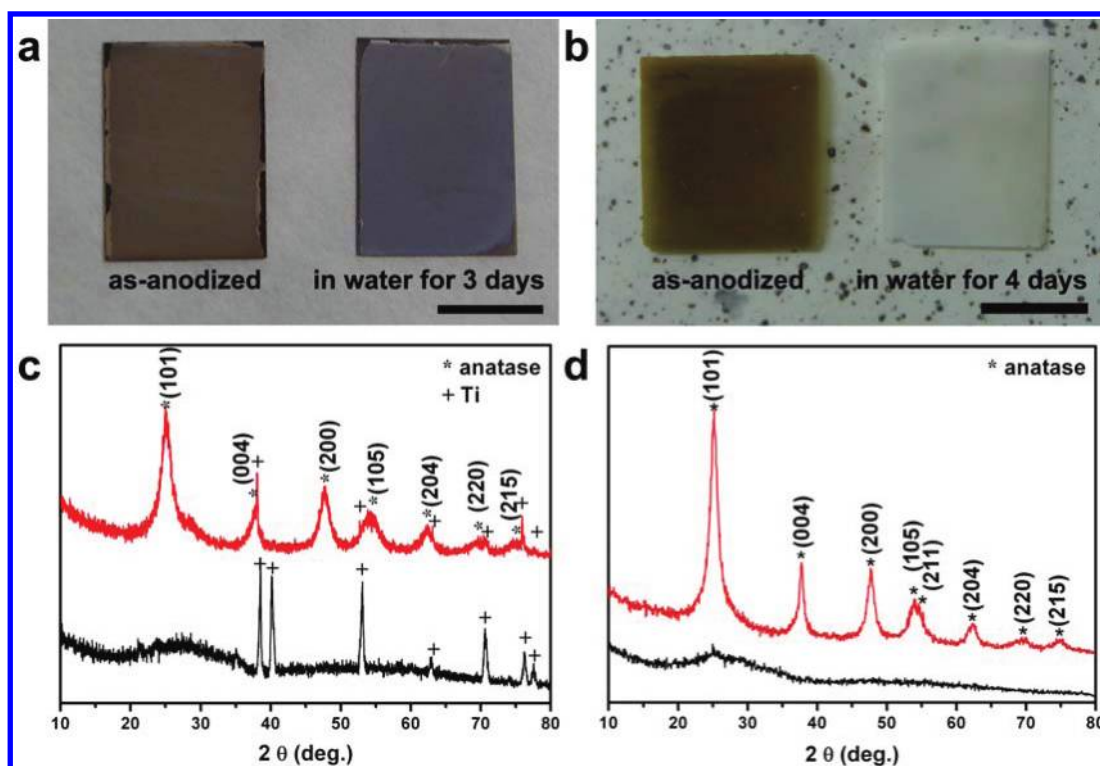
Figure 1. Appearance change and phase transformation of the anodized TiO_2 nanotube films before and after the water-soaking treatment. (a, b) Digital photographs showing the appearance change of a TiO_2 NT/Ti film and a free-standing TiO_2 NT membrane before and after the treatment. Scale bars: 1 cm. (c, d) XRD patterns demonstrating the phase transformation before (black line) and after (red line) the water soaking for (c) a TiO_2 NT/Ti film and (d) a free-standing TiO_2 NT membrane. The samples were soaked in deionized water at room temperature ($\sim$23 °C).

TiO_2 nanostructures to be more readily integrated with polymeric substrates or into some temperature-sensitive photoelectric devices.

Experimentally, the phase transformation can take place either in a TiO_2 NT film adhered to the Ti foil (TiO_2 NT/Ti) or in a free-standing TiO_2 NT membrane. The self-organized TiO_2 NTs were fabricated by anodizing Ti foils in a ethylene glycol electrolyte containing 0.5 wt % NH_4F and 2 wt % H_2O in a temperature range of 15—20 °C (see Supporting Information for more details). The free-standing, through-hole TiO_2 NT membranes can be obtained by an in situ separation method we developed recently.[32] After anodization, the samples were briefly rinsed with distilled water and then soaked into deionized water ($\geq$18 MΩ) at room temperature ($\sim$23 °C). Panels a and b of Figure 1 show the typical appearance change of a TiO_2 NT/Ti foil and a free-standing TiO_2 NT membrane before and after soaking in water for a certain time. It is seen that the as-anodized TiO_2 NT films are dark yellow, in line with many previous reports.[11,12] After the water-soaking treatment, the films decolorized and the visible appearance turned to white, a characteristic of crystalline TiO_2. X-ray diffractometry (XRD) studies disclose that the water soaking has successfully transformed the as-anodized amorphous TiO_2 NTs into a pure anatase phase (Figure 1c,d). The average crystallite size was estimated to be 6—7 nm according to the Scherrer equation.

The microscopic morphology of the TiO_2 nanostructures was examined by scanning electron microscopy (SEM). It was found that before evolving into anatase mesoporous TiO_2 NWs, the amorphous TiO_2 NTs underwent a novel morphological transformation as the water-soaking time increased, resulting in two distinct intermediate structures. Figure 2a,b exhibit representative

top-view and side-view SEM micrographs of the as-anodized TiO_2 NT arrays. Consistent with previous reports on top-porous TiO_2 NTs,[32,33] a porous layer with a thickness of hundreds of nanometers is observed on the top of the NT arrays, the morphology of which is analogous to that of porous anodic alumina.[34] After the top porous layer was scratched off, a close-packed array of discrete NTs was revealed (Figure 2a, inset).

From Figure 2b, it is seen that the as-anodized TiO_2 NTs have a smooth tube wall. After the sample was soaked in water over 15 h, many small particles with a particle size of $\sim$10 nm appeared on the top surface, as evident in Figure 2c. When the top porous layer was removed, it was observed that the original single-walled NTs had transformed into double-walled NTs. A cross-sectional SEM image taken from the lower part of the array also confirms the formation of double-walled NTs (Figure 2d). When the water-soaking time was increased to more than 25 h, more particles emerged on the top surface and the nanopores were nearly blocked (Figure 2e). Meanwhile, some bigger needle-like particles were also observed. Moreover, it was found that the underlying architectures had evolved from the doubled-walled NTs into a wire-in-tube architecture (Figure 2e, inset). Figure 2f shows a typical cross-sectional SEM micrograph of the array subjected to water soaking of 25 h, illustrating that the inner wires have a fairly rough surface and in some places the neighboring outer shells (i.e., tubes) coalesced. If one further prolongs the water-soaking time to over 3 days, "urchin-like" TiO_2 nanostructures will evolve on the top surface of the anodized film, and the original nanoporous morphology is not visible any more, as seen in Figure 2g (see Figure S1 in the Supporting Information for more details about the "urchins"). Correspondingly, it is found that all the
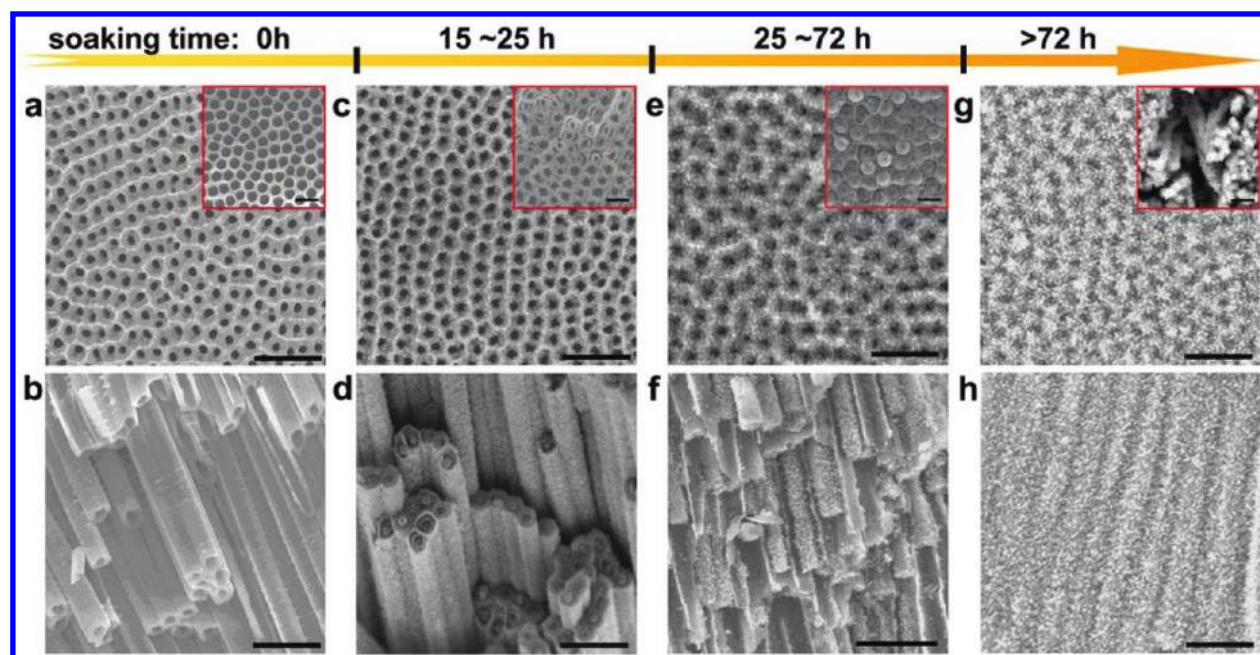
Figure 2. SEM characterization of the morphological evolution as a function of water-soaking time: (a, b) as-anodized TiO_2 nanotube arrays; (c, d) intermediate double-walled TiO_2 nanotube arrays obtained by water soaking for 15−25 h; (e, f) intermediate wire-in-tube TiO_2 nanoarchitectures formed by water soaking for 25−72 h; (g, h) mesoporous TiO_2 nanowire arrays obtained by a long-term water soaking (>72 h). Scale bars: 500 nm. The insets of panels a, c, e, and g denote the morphologies of the nanostructure arrays after scratching the top porous layer off. Scale bars: 200 nm.
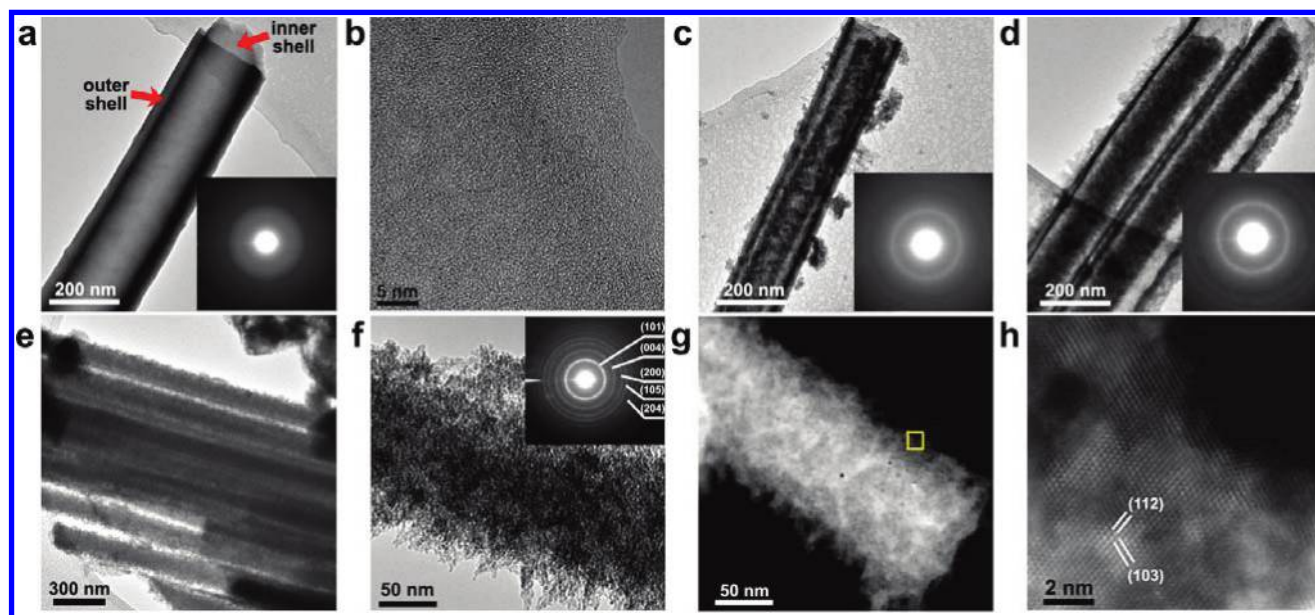

Figure 3. TEM characterization of TiO_2 nanostructures: (a) TEM micrograph of the as-anodized amorphous TiO_2 nanotubes, showing the two-layer structure of tube walls; (b) HRTEM image of the amorphous TiO_2 nanotubes; representative TEM micrographs of (c) the double-walled TiO_2 nanotubes, (d) wire-in-tube nanoarchitectures, and (e, f) mesoporous anatase nanowires; (g) HAADF STEM image of a single porous nanowire, clearly showing the mesoporous nature; (h) high-resolution STEM micrograph of the mesoporous nanowires taken from the rectangular area in (g), illustrating the well-defined crystalline nature. Insets of panels a, c, d, and f show corresponding electron diffraction patterns.

TiO_2 NTs have exclusively transformed into solid NWs covered with a large density of tiny needles (Figure 2g inset and Figure 2h).

To gain further insight into the microstructures of the resulting TiO_2 nanostructures, transmission electron microscopy (TEM) investigations were carried out. Figure 3a shows a representative TEM image of the as-anodized TiO_2 NTs, in which the hollow tubular-like structure with a smooth tube wall can be clearly seen. Note that the tube wall consists of two layers, in accordance with previous observations.[35,36] As will be discussed in the following section, the formation of double-walled NTs upon water soaking can be partly ascribed to the existence of this two-layer structure. We performed extensive electron diffraction (ED) analyses on

either a single NT or NT bundles and only detected diffuse ED patterns (Figure 3a, inset), which confirmed that the as-anodized NTs are amorphous. The amorphous nature was further verified by the high-resolution TEM (HRTEM) examination, which showed a homogeneous mazelike pattern without any detectable lattice fringes, an indication of amorphous materials (Figure 3b). Panels c and d of Figure 3 reveal the typical TEM micrographs of TiO_2 nanostructures obtained by water soaking for 18 and 36 h, respectively, unambiguously illustrating a double-walled tubular structure and a wire-in-tube architecture. Compared to the completely diffusive ED pattern shown in Figure 3a, one strong diffraction ring together with a few weak rings appear in the ED patterns taken from the double-walled NTs and wire-in-tube structures, implying that a spatial atomistic ordering is forming upon water soaking. However, the calculated lattice spacing according to the strongest diffraction was found to be $d = 3.81$ Å, which is a bit larger than $d_{(101)}$ of anatase TiO_2 (JCPDF 89-4921). This may suggest that the originally randomly distributed TiO_6^{2-} octahedra have rearranged themselves and are approaching to each other to share their edges (see the following section for detailed discussion). Figure 3e–h show the detailed microstructural characterization of the TiO_2 nanostructures obtained by a long-term water soaking. It is seen that the hollow tubular morphology is not visible any more. Instead, solid NWs with numerous tiny needles on their surfaces were observed. The ED pattern taken from these NWs exhibits a set of well-defined rings, which can be indexed as anatase TiO_2 (Figure 3e, inset) and is consistent with the above XRD results (Figure 1). Upon closer examination of the NWs, it was found that the NWs contain a great number of mesopores with a mean pore size of ∼3.2 nm (Figure 3f). Figure 3g reveals a typical high angle annular dark field (HAADF) scanning transmission electron microscopy (STEM) micrograph of a single TiO_2 NW, in which the mesoporous nature can be seen more clearly. The high-resolution STEM study demonstrated that the mesoporous NWs are well-crystallized, as shown in Figure 3h, from which the lattice fringes of anatase {103} and {112} crystal planes can be distinguished. Nevertheless, a certain amount of amorphous TiO_2 can still be found in the NWs, suggesting the amorphous anatase transformation was incomplete (Figure S2, Supporting Information).

To examine the universality of the room temperature water-driven amorphous-anatase phase transformation, we prepared amorphous TiO_2 powders by the hydrolysis of $Ti[OCH(CH_3)_2]_4$ and performed similar water-soaking treatments (Supporting Information). It was found that the amorphous TiO_2 powders started crystallizing after soaking in water at room temperature for 2 days, and the size of crystallites was gradually increased with the increasing soaking time up to 9 days, amounting to ∼7.5 nm (Figure S3, Supporting Information). However, the crystallized powders were not phase-pure anatase but contained a fraction of brookite. The formation of brookite phase can be suppressed by adding little NH_4F into water, in which case only pure anatase was obtained (Figure S4, Supporting Information).

It is well-known that TiO_6^{2-} octahedra are basic building blocks of all polymorphs of TiO_2 (i.e., amorphous, anatase, rutile, and brookite). The structural rearrangement of the TiO_6^{2-} octahedral units in the amorphous TiO_2 induced by their surface environment is believed to play an essential role in the crystallization of amorphous TiO_2 to anatase.[37−40] Since water is the only substance involved in this amorphous-anatase phase transformation, we believe that the phase transformation process is spontaneous in water. First, water molecules form bridges between surface hydroxyl groups of two different octahedra that share one common vertex, using the two lone pairs of electrons on the oxygen (Figure 4a, step 1). Subsequent dehydration will lead to the linkage of two octahedra by sharing their edges, as schematically illustrated in Figure 4a (step 2). The addition of the third octahedron driven by water will proceed in such a fashion that the three octahedra are linked by sharing edges in a right angle (Figure 4a, step 3), thus forming a basic unit of anatase. It is believed that a linear chain of aligned octahedra (the basic units of rutile) is unlikely formed under the present experimental condition, because it has been demonstrated both theoretically and experimentally that in a neutral or weak acid solution the Gibbs free energy of rutile clusters is higher than that of anatase ones[39] and therefore anatase nuclei should be more thermodynamically stable. The formed right-angle octahedron assembly will then connect with another identical assembly by sharing edges, thus forming a unit cell of anatase (Figure 4a, step 4). It is assumed that the crystallization of amorphous TiO_2 will proceed via a dissolution−precipitation process, in which randomly distributed TiO_6^{2-} octahedra are dissolved and rearrange themselves driven by water, and then precipitate as the anatase phase starts nucleating. Accompanying the dissolution−precipitation, numerous mesopores are also formed.

It is believed that the distinctive morphology transformation should be closely related to the phase transformation process and is determined by the unique geometrical configuration of the TiO_2 NT arrays as well as the two-layer structure of the tube walls (Figure 3a). On the one hand, as shown in Figure 4b, the relatively large space inside the NTs (varying from 60 to 100 nm) allows sufficient water molecules to access the inner surface of the tubes to drive nucleation and growth of the anatase phase (i.e., the dissolution−precipitation process). By contrast, the narrow space between the adjacent TiO_2 NTs (a few nanometers) in conjunction with the porous layer on the top surface (Figure.1) greatly limits the diffusion and transport of water so that the dissolution−precipitation of the outer surface of the NTs occurs very slowly. Hence, the dissolution−precipitation of TiO_2 in the inner shell of tube walls is more kinetically favorable and will progressively proceed inward (Figure 4b, stage 1). On the other hand, it is assumed that the inner shell is intrinsically more prone to be dissolved as it is less compact than the outer shell.[35,36] In this case, the dissolution−precipitation rate will drastically decrease once the dissolution−precipitation process is complete in the inner shell. This would lead to a separation of the inner shell from the outer shell, forming the double-walled NTs (Figure 4b, stage 2). Afterward, water will move into the space between the inner tube and outer tube and further accelerate the dissolution−precipitation in both of them. Because the outer tube is relatively more compact and less prone to be dissolved upon water attack, a wire-in-tube architecture is gradually formed (Figure 4b, stage 3). However, if the water-soaking time is further prolonged, the outer tubes will finally disappear upon dissolution−precipitation and nanowires can be exclusively obtained (Figure 4b, stage 4). As mentioned above, the constant dissolution−precipitation during the phase and morphology transformations will give rise to the formation of a great number of mesoscopic pores, yielding a marked increase in surface area. Time-dependent phase and morphology investigations revealed that the as-obtained mesoporous anatase NWs are kinetically stable under the present experimental conditions (i.e., water, room temperature), whose phase, crystallinity and mesoporous morphology show no discernible change with the prolonged soaking time up to 1 month. This
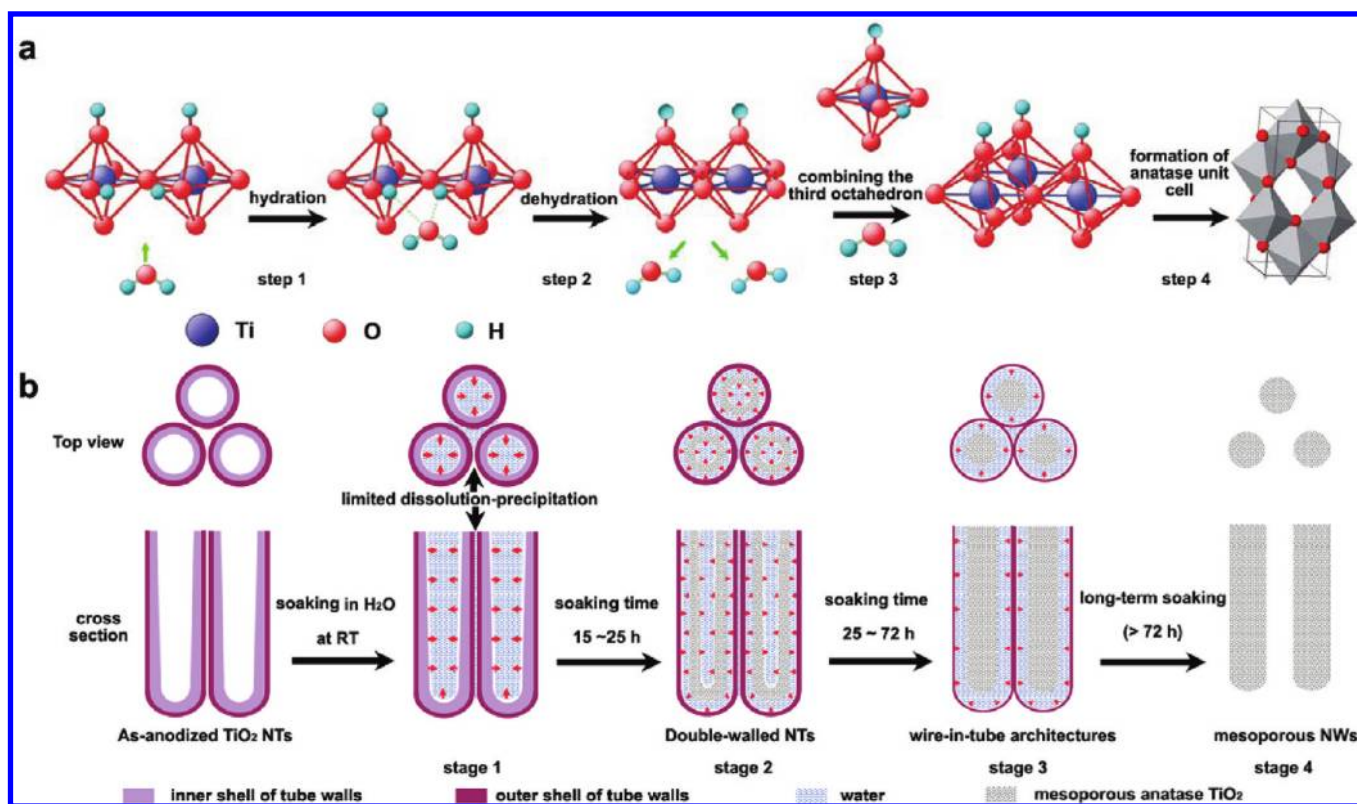
Figure 4. Phase and morphology transformation mechanisms. (a) A schematic showing the nucleation of anatase from amorphous TiO_2 induced by water. (b) A scheme illustrating the morphology transformation of the as-anodized TiO_2 nanotubes upon water soaking. The red arrows denote the direction along which the dissolution−precipitation of TiO_6^{2-} octahedra proceeds.

could be explained by the fact that anatase is a thermodynamically stable phase, and the TiO_6^{2-} octahedra in anatase are not liable to be dissolved in water at room temperature.

It is noted that although considerable efforts have been dedicated to improving the surface area of TiO_2 NT arrays by adjusting the tube diameter, wall thickness, etc., the maximum surface area of anodized TiO_2 NTs achieved so far for crystalline NTs is only about 35−40 m^2 g^{-1},[41] according to N$_2$ adsorption/desorption measurements (Figure 5a). In contrast, the mesoporous NWs obtained by long-term water-soaking treatment of amorphous TiO_2 NTs exhibit a surface area as high as 203.3 m^2 g^{-1}, which is about 5.5 times larger than that of the thermally annealed (anatase) TiO_2 NTs. Their pore size distribution analyzed by the Barrett−Joyner−Halenda (BJH) method is 3.73 nm, close to the TEM observations.

The photocatalytic performance of the mesoporous anatase NWs toward hydrogen generation from water was evaluated and compared with that of as-anodized amorphous TiO_2 NTs and thermally annealed TiO_2 NTs (500 °C in air, 3 h), as shown in Figure 5b. In our experiment, 10 vol % methanol was added as the sacrificial agent into the water, and 1 wt % of Pt was in situ photodeposited onto/into TiO_2 samples as cocatalyst (see Supporting Information for more details). The typical morphology of the Pt nanoparticle loaded mesoporous anatase NWs is shown in Figure S5 (Supporting Information), which reveals that most mesopores are still accessible without blocking by Pt nanoparticles. According to Figure 5b, the amorphous TiO_2 NTs only exhibit a negligible catalytic activity for hydrogen generation. The thermally annealed TiO_2 NTs reveal a better performance, having a hydrogen evolution rate of 248.3 μmol g^{-1} h^{-1}. By contrast, the

mesoporous anatase TiO_2 NWs obtained by a simple water-soaking treatment show a hydrogen evolution rate as high as 480 μmol g^{-1} h^{-1}, about 1.9 times higher than that of well-crystallized TiO_2 NTs obtained by thermal annealing. However, the 1.9 times enhancement in photocatalytic activity for the mesoporous anatase NWs cannot be fully accounted for by the improved surface area, because the surface area of the mesoporous NWs is 5.5 times higher than that of the thermally annealed TiO_2 NTs, as mentioned above. The mismatch can be explained by the fact that the mesoporous anatase NWs have a lower degree of crystallinity (i.e., small crystallite size) and a higher density of defects which will compromise the possible photocatalytic activity enhancement arising from the surface area improvement. Nevertheless, it is expected that the photocatalytic performance of the mesoporous anatase NWs could be further improved upon optimization of the water-soaking process.

It is also worth mentioning that for a longer term photocatalytic reaction (up to 60 h), we observed that the photocatalytic performance of the as-anodized amorphous TiO_2 NTs increases with reaction time, as shown in Figure S6 (Supporting Information). This may be related to the fact that the amorphous TiO_2 NTs had in situ transformed into mesoporous anatase NWs during the photocatalytic reaction, which was confirmed by XRD examination of the sample after reaction (Figure S7, Supporting Information). A systematic study on how the morphology, microstructure, and photocatalytic activity of both amorphous TiO_2 NTs and water-soaked samples evolve during the photocatalytic reaction is under investigation.

In summary, we have demonstrated that the amorphous-anatase phase transformation of titania can be realized at room
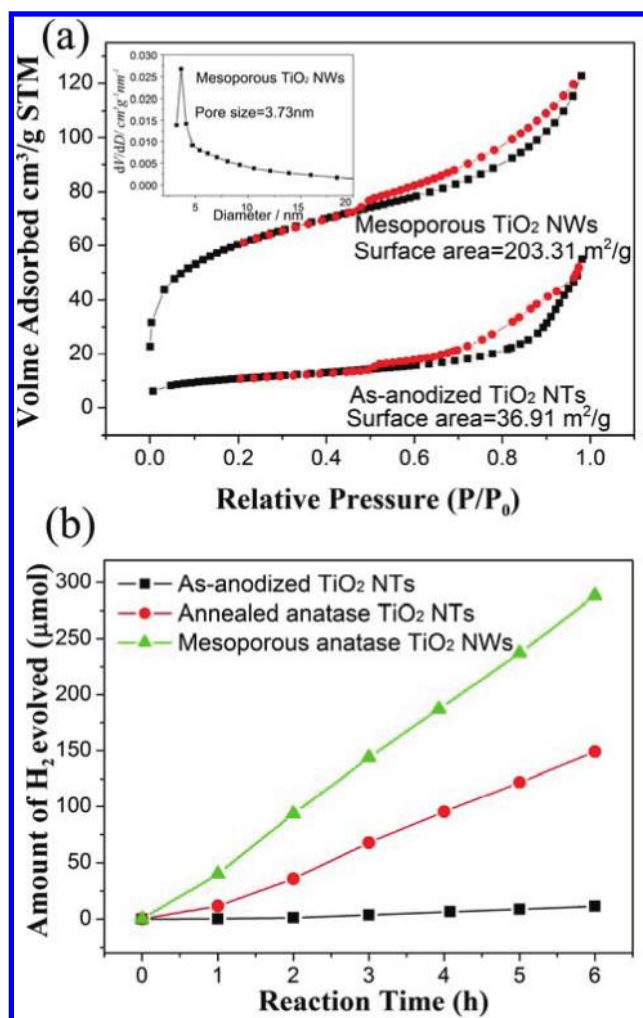
Figure 5. (a) N_2 absorption/desorption isotherms of the thermally annealed anatase TiO_2 NTs and anatase mesoporous TiO_2 NWs. Inset: pore size distribution profile of the mesoporous TiO_2 NWs. (b) Photocatalytic hydrogen-generation performance of the obtained mesoporous anatase TiO_2 NWs, as-anodized amorphous TiO_2 NTs, and thermally annealed anatase TiO_2 NTs. The thermal annealing was carried out in air at 500 °C for 3 h.

when the amorphous titania nanotubes are used in some special cases like drug delivery and nanoelectronic devices.

ASSOCIATED CONTENT

S **Supporting Information.** Experimental details and additional figures showing TEM micrographs of TiO_2, time-dependent phase evolution if TiO_2 powders, influence of F^- ions on the phase composition of the resulting crystalline TiO_2, photocatalytic hydrogen-generation performance of the amorphous TiO_2 NTs, and XRD patterns of the as-anodized amorphous TiO_2 NTs. This material is available free of charge via the Internet at http://pubs.acs.org.

AUTHOR INFORMATION

Corresponding Author

*E-mail: dwang@chemsys.t.u-tokyo.ac.jp (D. Wang); lifeng.liu@inl.int (L. Liu).

Author Contributions

$^{\parallel}$These authors contributed equally to this work.

REFERENCES

(1) O'Regan, B.; Grätzel, M. *Nature* **1991**, *353*, 737–740.
(2) Law, M.; Greene, L. E.; Johnson, J. C.; Saykally, R.; Yang, P. D. *Nat. Mater.* **2005**, *4*, 455–459.
(3) Gur, I.; Fromer, N. A.; Geier, M. L.; Alivisatos, A. P. *Science* **2005**, *310*, 462–465.
(4) Maeda, K.; Teramura, K.; Lu, D. L.; Takata, T.; Saito, N.; Inoue, Y.; Domen, K. *Nature* **2006**, *440*, 295.
(5) Tian, B. Z.; Zheng, X. L.; Kempa, T. J.; Fang, Y.; Yu, N. F.; Yu, G. H.; Huang, J. L.; Lieber, C. M. *Nature* **2007**, *449*, 885–888.
(6) Wang, X. C.; Meada, K.; Thomas, A.; Takanabe, K.; Xin, G.; Carlsson, J. M.; Domen, K.; Antonietti, M. *Nat. Mater.* **2009**, *8*, 76–80.
(7) Osterloh, F. E. *Chem. Mater.* **2008**, *20*, 35–54.
(8) Hernandez-Alonso, M. D.; Fresno, F.; Suarez, S.; Coronado, J. M. *Energy Environ. Sci.* **2009**, *2*, 1231–1257.
(9) Fujishima, A.; Honda, K. *Nature* **1972**, *238*, 37–38.
(10) Liu, G.; Wang, L. Z.; Yang, H. G.; Cheng, H. M.; Lu, G. Q. *J. Mater. Chem.* **2010**, *20*, 831–843.
(11) Mor, G. K.; Varghese, O. K.; Paulose, M.; Shankar, K.; Grimes, C. A. *Sol. Energy Mater. Sol. Cells* **2006**, *90*, 2011–2075.
(12) Wang, D. A.; Yu, B.; Wang, C. W.; Zhou, F.; Liu, W. M. *Adv. Mater.* **2009**, *21*, 1964–1967.
(13) Kuang, D.; Brillet, J.; Chen, P.; Takata, M.; Uchida, S.; Miura, H.; Sumioka, K.; Zakeeruddin, S. M.; Grätzel, M. *ACS Nano* **2008**, *2*, 1113–1116.
(14) Mor, G. K.; Shankar, K.; Paulose, M.; Varghese, O. K.; Grimes, C. A. *Nano Lett.* **2006**, *6*, 215–218.
(15) Albu, S. P.; Ghicov, A.; Macak, J. M.; Hahn, R.; Schmuki, P. *Nano Lett.* **2007**, *7*, 1286–1289.
(16) Zhu, K.; Neale, N. R.; Miedaner, A.; Frank, A. J. *Nano Lett.* **2007**, *7*, 69–74.
(17) Feng, X. J.; Shankar, K.; Varghese, O. K.; Paulose, M.; Latempa, T. J.; Grimes, C. A. *Nano Lett.* **2008**, *8*, 3781–3786.
(18) Varghese, O. K.; Paulose, M.; Grimes, C. A. *Nat. Nanotechnol.* **2009**, *4*, 592–597.
(19) Mor, G. K.; Shankar, K.; Paulose, M.; Varghese, O. K.; Grimes, C. A. *Nano Lett.* **2005**, *5*, 191–195.
(20) Richter, C.; Schmuttenmaer, C. A. *Nat. Nanotechnol.* **2010**, *5*, 769–772.
(21) Kang, T. S.; Smith, A. P.; Taylor, B. E.; Durstock, M. F. *Nano Lett.* **2009**, *9*, 601–606.

temperature only with the assistance of water. This approach offers a facile, scalable, cost-effective, and energy-saving solution for obtaining photoactive anatase from amorphous TiO_2, which would be of particular industrial interest. Moreover, for the anodized titania nanotubes, this novel phase transformation can also simultaneously induce a morphology transformation, yielding mesoporous nanowires having markedly enlarged surface areas. These anatase mesoporous nanowires exhibit a pronouncedly enhanced photocatalytic activity toward hydrogen evolution, about 1.9 times higher than that of the well-crystallized TiO_2 NTs obtained by thermal annealing. We believe that the spontaneous phase and morphology transformations reported here will open up a new pathway for the morphology and crystallinity control of TiO_2 nanostructures and will have considerable potential for the development of high-performance, low-cost dye-sensitized solar cells, photocatalysts, and lithium-ion batteries. In addition, our study also suggests that the long-term stability in the presence of aqueous solution has to be carefully considered

(22) Sauvage, F.; Fonzo, F. D.; Bassi, A. L.; Casari, C. S.; Russo, V.; Divitini, G.; Ducati, C.; Bottani, C. E.; Comte, P.; Graetzel, M. *Nano Lett.* **2010**, *10*, 2562–2567.

(23) Bang, J. H.; Kamat, P. V. *Adv. Funct. Mater.* **2010**, *20*, 1970–1976.

(24) Varghese, O. K.; Gong, D. W.; Paulose, M.; Grimes, C. A.; Dickey, E. C. *J. Mater. Res.* **2003**, *18*, 156–165.

(25) Yu, J. G.; Dai, G. P.; Cheng, B. *J. Phys. Chem. C* **2010**, *114*, 19378–19385.

(26) Allam, N. K.; Shankar, K.; Grimes, C. A. *Adv. Mater.* **2008**, *20*, 3942–3946.

(27) Allam, N. K.; Grimes, C. A. *Langmuir* **2009**, *25*, 7234–7240.

(28) Crepaldi, E. L.; Soler-Illia, G. J.; de, A. A.; Grosso, D.; Cagnol, F.; Ribot, F.; Sanchez, C. *J. Am. Chem. Soc.* **2003**, *125*, 9770–9786.

(29) Wang, D.; Zhou, F.; Wang, C.; Liu, W. *Microporous Mesoporous Mater.* **2008**, *116*, 658–664.

(30) Liu, B.; Zeng, H. *Chem. Mater.* **2008**, *20*, 2711–2718.

(31) Zukalová, M.; Zukal, A.; Kavan, L.; Nazeeruddin, M. K.; Liska, P.; Grätzel, M. *Nano Lett.* **2005**, *5*, 1789–1792.

(32) Wang, D. A.; Liu, L. F. *Chem. Mater.* **2010**, *22*, 6656–6664.

(33) Wang, D.; Liu, Y.; Yu, B.; Zhou, F.; Liu, W. *Chem. Mater.* **2009**, *21*, 1198–1206.

(34) Liu, L. F.; Lee, S. W.; Li, J. B.; Alexe, M.; Rao, G. H.; Zhou, W. Y.; Lee, J. J.; Lee, W.; Gösele, U. *Nanotechnology* **2008**, *19*, 495706.

(35) Albu, S. P.; Ghicov, A.; Aldabergenova, S.; Drechsel, P.; LeClere, D.; Thompson, G. E.; Macak, J. M.; Schmuki, P. *Adv. Mater.* **2008**, *20*, 4135–4139.

(36) Su, Z. X.; Zhou, W. Z. *J. Mater. Chem.* **2009**, *19*, 2301–2309.

(37) Yanagisawa, K.; Ovenstone, J. *J. Phys. Chem. B* **1999**, *103*, 7781–7787.

(38) Yin, H. B.; Wada, Y.; Kitamura, T.; Kambe, S.; Murasawa, S.; Mori, H.; Yanagida, S. *J. Mater. Chem.* **2001**, *11*, 1694–1703.

(39) Finnegan, M. P.; Zhang, H. Z.; Banfield, J. F. *J. Phys. Chem. C* **2007**, *111*, 1962–1968.

(40) Barnard, A. S.; Curtiss, L. A. *Nano Lett.* **2005**, *5*, 1261–1266.

(41) Paulose, M.; Prakasam, H. E.; Varghese, O. K.; Peng, L.; Popat, K. C.; Mor, G. K.; Desai, T. A.; Grimes, C. A. *J. Phys. Chem. C* **2007**, *111*, 14992–14997.